E3S Web of Conferences **601**, 00027 (2025) https://doi.org/10.1051/e3sconf/202560100027
ICEGC'2024

Comparative study of conventional sliding mode control and integral sliding mode control for a bidirectional dc-dc converter in an electric vehicle charger

Khadija Oualifi[1,*], *Hassan* Abouobaida[1], *Youssef* Mchaouar[1], *Abdelmoghit* Fathelkhair[1], *Hajar* Akli[1], and *Younes* Abouelmahjoub[1]

[1]LabSIPE at National School of Applied Sciences, Chouaib Doukkali University, EL Jadida 24002, Morocco

Abstract. Bidirectional dc-dc converters are crucial for integrating electric vehicles (EVs) with the electrical grid, facilitating both grid-to-vehicle (G2V) and vehicle to grid (V2G) energy transfers. Nonetheless, effectively controlling bidirectional energy flow poses significant challenges. This study compares two control methods, the conventional sliding mode controller (CSMC) and the integral sliding mode controller (ISMC), as applied to a bidirectional dc-dc converter. The dc-dc converter functions in two distinct modes: during grid to vehicle (G2V), it operates in buck mode to charge the battery using either constant current or constant voltage based on the battery's voltage level; and during vehicle-to-grid (V2G), it switches to boost mode to discharge battery power into the grid at a constant current. The proposed controllers were simulated using MATLABK/Simulink and compared with a traditional linear PI controller. The simulation results highlight the efficiency and superiority of ISMC over both CSMC and PI control. In particular, ISMC offers superior performance in terms of response time and accuracy.

1 Introduction

The advancement and innovation in battery electric vehicles (BEVs) are actively shaping and progressing within the forefront of the automotive industry [1]. However, the growing integration of battery electric vehicles (BEVs) is posing challenges to the power grid by increasing demand for electricity. On the other hand, BEVs also represent potential assets for the grid that can be beneficial if managed effectively [2]. The concept of Vehicle-to-X (V2X) indeed holds significant promise for the future of electric vehicles (EVs) and energy management. V2X technology enables the transfer of power between vehicles and various external devices or systems, offering several potential applications: Vehicle-toLoad (V2L), Vehicle-to-Home (V2H) and Vehicle-to-Grid (V2G) [3-4]. Electric vehicle charging infrastructure must be well-suited to support the needs of electric vehicles. Chargers can be categorized based on factors such as how energy is transferred (conductive and inductive), the power levels for charging (off-board or stationary chargers and on-board chargers), and the direction of energy flow (unidirectional and bidirectional chargers) [5]. An electric vehicle (EV) charger generally consists of two converters: an AC-DC converter for power factor

*e-mail: Oualifi.k@ucd.ac.maauthor

correction and a DC-DC converter for battery connection [6]. Conventional electric vehicle chargers are generally equipped with unidirectional converters designed primarily for grid-to-vehicle (G2V) charging. However, to support vehicle-to-anything (V2X) technologies such as vehicle-to-grid (V2G), vehicle-to-home (V2H) and vehicle-to-charge (V2L), it is essential to incorporate bidirectional converters capable of handling sufficient power [7-8]. During grid-to-vehicle (G2V) mode, the AC-DC converter rectifies AC power to DC, while the DC-DC converter steps down the voltage for charging the vehicle's battery. In vehicle-to-grid (V2G) mode, the AC-DC converter operates as an inverter to convert DC power from the vehicle's battery to AC, while the DC-DC converter steps up the voltage to match the grid's requirements for feeding power back into the grid [8]. Effective control strategies are crucial for electric vehicle (EV) chargers to ensure they can respond quickly and robustly to disturbances and changes in operating conditions. In the literature, several approaches are used, including controllers such as Integral Proportional (IP) controllers [9-10], Linear Quadratic Regulators (LQR) [11]. These controllers are generally designed on the basis of a linearized model of the system around a nominal operating point. They yield favorable outcomes when the system operates within a narrow margin around this nominal point. However, in the context of vehicle-to-grid (V2G) electric vehicle battery chargers (BEVs), the operating conditions can vary significantly, especially during transitions between grid-to-vehicle (G2V) and V2G modes. These transitions can cause rapid changes in system dynamics, leading to deviations from the nominal operating conditions. Linear controllers may face challenges in maintaining satisfactory performance under such dynamic conditions, primarily because they are designed based on linear models. Similarly, intelligent control systems have been developed in references [12-13]. These controllers typically rely on large datasets for learning and may require significant computing resources, particularly in real-time applications. In addition, the opaque nature of some artificial intelligence techniques can limit interpretability and robustness in specific situations. This is where non-linear control strategies such as sliding-mode non-linear control come in [14-16]. It can stabilize the system over a wide range of operating conditions, making it particularly suitable for applications such as electric vehicle battery chargers, where operating conditions can vary considerably. This study undertakes a comparative analysis between conventional sliding-mode control and integral-action sliding-mode control applied to a DC-DC bidirectional power converter. The aim is to achieve efficient regulation of battery voltage and current, thereby ensuring safe and effective charging and discharging operations in both grid-to-vehicle (G2V) and vehicle-to-grid (V2G) modes. The paper is organized as follows: Section 1 introduces the context of this work. Section 2 provides detailed descriptions of the topology and its controls. Section 3 presents the design and simulation results using MATLAB/Simulink for the studied AC/DC converter and its control strategies. Section 4 concludes the paper.

2 Description of the proposed system and its controls

The schematic of bidirectional on-board chargers for electric vehicle batteries, depicted in Fig.1, includes two bidirectional power stages: ACDC and DCDC. The previous study has addressed the AC-DC bidirectional converter and its control [17]. In the following work, our focus will be on the control of the DC-DC section.

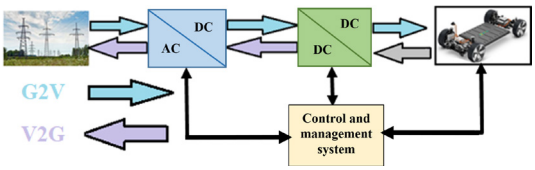

Figure 1. Schematic block diagram of a bidirectional electric vehicle charging station

2.1 DC-DC power converter

The electrical diagram of the DC-DC converter linked with the battery is depicted in Fig. 2. The bidirectional DC-DC converter comprises two switches, S1 and S2, an inductor L0

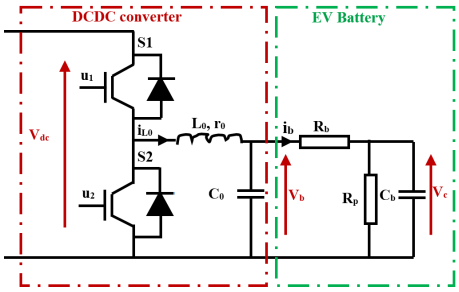

Figure 2. Electrical schematic of the bidirectional DC-DC power converter.

with internal resistance r0, and a filter capacitor C0 [18-19]. This converter serves as an interface between the DC bus and the battery, capable of operating in two modes: buck mode for charging the battery and boost mode for discharging stored energy from the battery to the grid. The battery is modelled using the equivalent series resistance (ESR), denoted by Rb, and the equivalent parallel resistance (EPR), denoted by Rp, with Cb indicating the battery capacity [20-22]. And finally, u1 and u2 denote the switch control signals generated by the PWM block. Applying Kirchhoff's laws to the electrical circuit in Fig. 2 yields the following instantaneous model.

$$L_0 \frac{di_{L0}}{dt} = -r_0 i_{L0} - V_b + \mu_{12} V_{dc} \tag{1}$$

$$C_0 \frac{dV_b}{dt} = i_{L0} - \frac{V_b - V_c}{R_b} \tag{2}$$

$$C_b \frac{dV_c}{dt} = \frac{V_b - V_c}{R_b} - \frac{V_c}{R_P} \tag{3}$$

Where u12= (Su1 + (1-S) (1-u2)), S is the switching variable between buck mode and boost mode for the DC-DC converter. For controller design, using the averaged model (4-6), ob-

tained by averaging models (1-3) over a switching period [23], is more practical.

$$\dot{x}_1 = -\frac{r_0}{L_0}x_1 - \frac{1}{L_0}x_2 + \frac{U_{12}}{L_0}V_{dc} \tag{4}$$

$$\dot{x}_2 = \frac{1}{C_0}x_1 - \frac{1}{R_bC_0}x_2 + \frac{1}{R_bC_0}x_3 \tag{5}$$

$$\dot{x}_3 = \frac{1}{R_bC_b}x_2 - \left(\frac{1}{R_bC_b} + \frac{1}{R_PC_b}\right)x_3 \tag{6}$$

Where, x_1, x_2, and x_3 represent the average values of the current (i_{L0}), the battery terminal voltage (V_b), and the internal battery voltage (V_c), respectively. μ_{12} is the average value of u_{12}.

2.2 Controller design

In this paper, the bidirectional DC-DC converter controllers are designed to charge and discharge the battery safely and efficiently during G2V and V2G modes respectively. Consequently, the CC-CV (constant current - constant voltage) charging method [24-26] is adopted during the G2V phase, while the CC method is adopted during the V2G phase with a negative reference. The depicted CC-CV charging profile is illustrated in Fig. 3. The CC stage controller is programmed to regulate the battery current (Ib) to match its reference value, Ibref. This current remains fixed and constant until the battery voltage reaches Vbref, a predetermined limit. Once reaching Vbref, the charger transitions to the constant voltage (CV) stage to safely complete the charging process without risking overcharge. During the CV phase, the CV controller ensures that the battery voltage, Vb, aligns with its reference, VBref. Throughout this stage, the charging current gradually decreases until it reaches the cut-off current, ICO.

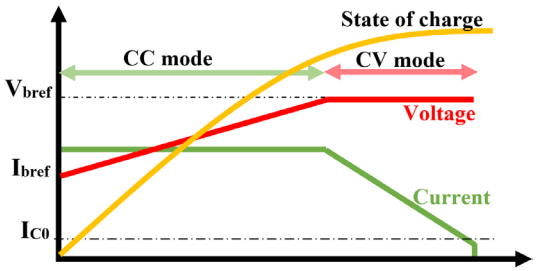

Figure 3. CC-CV charging profile.

2.2.1 Conventional sliding mode controller (CSMC)

CC stage controller design
From subsystem Eqs. (4-6), it is evident that designing the control involves computing the double derivative of the error between ib and its reference. The battery current error is defined as follows:

$$e_1 = i_b - I_{bref} \tag{7}$$

$$i_b = \frac{x_2 - x_3}{R_b} \tag{8}$$

The first and second time derivatives of e1 in equation (7) are calculated by setting the derivative of Ibref to zero.

$$\dot{e}_1 = \frac{\dot{x}_2 - \dot{x}_3}{R_b} \tag{9}$$

$$\ddot{e}_1 = \frac{\ddot{x}_2 - \ddot{x}_3}{R_b} = \frac{1}{R_b C_0}\dot{x}_1 - \frac{a}{R_b}\dot{x}_2 + \frac{b}{R_b}\dot{x}_3 \tag{10}$$

$$\begin{cases} a = \frac{1}{R_b C_0} + \frac{1}{R_b C_b} \\ b = a + \frac{1}{R_P C_b} \end{cases} \tag{11}$$

The sliding surface can be chosen as follows:

$$s_1 = \dot{e}_1 + c_1 e_1 \tag{12}$$

Where c_1 represents the parameter of the sliding surface, a positive real constant. Deriving equation (12), we get

$$\dot{s}_1 = \ddot{e}_1 + c_1 \dot{e}_1 \tag{13}$$

To analyze stability, we utilize the following Lyapunov function:

$$V_1 = \frac{1}{2} s_1^2 \tag{14}$$

Taking the time derivative of Eq. (14), we get:

$$\dot{V}_1 = \dot{s}_1 s_1 \tag{15}$$

According to equations (9), (10), (13), and (15), we get:

$$\dot{V}_1 = s_1 \left(\frac{1}{R_b C_0}\dot{x}_1 + \frac{(c_1 - a)}{R_b}\dot{x}_2 - \frac{(c_1 - b)}{R_b}\dot{x}_3 \right) \tag{16}$$

To ensure the Lyapunov function's derivative is negative, it is necessary to impose the following constraint:

$$\frac{1}{R_b C_0}\dot{x}_1 + \frac{(c_1 - a)}{R_b}\dot{x}_2 - \frac{(c_1 - b)}{R_b}\dot{x}_3 = -k_1 \frac{s_1}{|s_1| + \alpha} \tag{17}$$

where k_1 and α are positive constants. By substituting the values of $\dot{x}_1$, $\dot{x}_2$, and $\dot{x}_3$ from Eqs. (4), (5), and (6) into Eq. (17), we can derive the global controller U_{12_SMC} for the CC stage as follows:

$$U_{12\_SMC} = \frac{C_0 L_0}{V_{dc}} \left(-R_b k_1 \frac{s_1}{|s_1| + \alpha} + a_1 x_1 + a_2 x_2 + a_3 x_3 \right) \tag{18}$$

Where

$$\begin{cases} a_1 = \frac{1}{C_0}\frac{r_0}{L_0} - (c_1 - a)\frac{1}{C_0} \\ a_2 = \frac{1}{C_0 L_0} + (c_1 - a)\frac{1}{R_b C_0} + (c_1 - b)\frac{1}{R_b C_b} \\ a_3 = -(c_1 - a)\frac{1}{R_b C_0} - (c_1 - b)\left(\frac{1}{R_b C_b} + \frac{1}{R_P C_b}\right) \end{cases} \tag{19}$$

The corresponding equivalent ($U_{12\_eq\_SMC}$) and switching ($U_{12\_sw\_SMC}$) controllers can be defined from Eq. (18) as follows:

$$U_{12\_eq\_SMC} = \frac{C_0 L_0}{V_{dc}} (a_1 x_1 + a_2 x_2 + a_3 x_3) \tag{20}$$

$$U_{12\_sw\_SMC} = -\frac{C_0 L_0}{V_{dc}} \left(R_b k_1 \frac{s_1}{|s_1| + \alpha} \right) \tag{21}$$

CV stage controller design
The battery voltage error can be define as bellows.

$$e_2 = x_2 - V_{bref} \tag{22}$$

The first and second time derivatives of e_2 from Eq. (22), when the value of $\dot{V}_{bref}$ is equal to zero:

$$\dot{e}_2 = \dot{x}_2 \tag{23}$$

$$\ddot{e}_2 = \ddot{x}_2 = \frac{1}{C_0}\dot{x}_1 - \frac{1}{R_b C_0}\dot{x}_2 + \frac{1}{R_b C_0}\dot{x}_3 \tag{24}$$

The sliding surface can be chosen as follows:

$$s_2 = \dot{e}_2 + c_2 e_2 \tag{25}$$

Where c_2 is the parameter of the sliding surface, which is a positive real constant. Taking the derivative of Eq. (25), we obtain:

$$\dot{s}_2 = \ddot{e}_2 + c_2 \dot{e}_2 \tag{26}$$

For stability analysis, the Lyapunov function is defined as follows:

$$V_2 = \frac{1}{2} s_2^2 \tag{27}$$

Deriving equation (27), we get:

$$\dot{V}_2 = \dot{s}_2 s_2 \tag{28}$$

According to equations (23), (24), (26), and (28), we get:

$$\dot{V}_2 = s_2 \left(\frac{1}{C_0}\dot{x}_1 + \left(c_2 - \frac{1}{R_b C_0} \right) \dot{x}_2 + \frac{1}{R_b C_0}\dot{x}_3 \right) \tag{29}$$

In order to respect the Lyapunov condition, we must apply the following constraint:

$$\frac{1}{C_0}\dot{x}_1 + \left(c_2 - \frac{1}{R_b C_0} \right) \dot{x}_2 + \frac{1}{R_b C_0}\dot{x}_3 = -k_2 \frac{s_2}{|s_2| + \alpha} \tag{30}$$

By substituting the values of $\dot{x}_1$, $\dot{x}_2$, and $\dot{x}_3$ from Eqs. (4), (5), and (6) into Eq. (30), we can derive the global controller U_{12} for the CV stage as follows:

$$U_{12\_SMC} = \frac{C_0 L_0}{V_{dc}} \left(-k_2 \frac{s_2}{|s_2| + \alpha} + b_1 x_1 + b_2 x_2 + b_3 x_3 \right) \tag{31}$$

Where

$$\begin{cases} b_1 = -\left(c_2 - \frac{1}{R_b C_0} \right) \frac{1}{C_0} + \frac{r_0}{C_0 L_0} \\ b_2 = \frac{1}{C_0 L_0} + (c_2 - a) \frac{1}{R_b C_0} \\ b_3 = \frac{1}{R_b C_0} (b - c_2) \end{cases} \tag{32}$$

The corresponding equivalent (U_{12_eq}) and switching (U_{12_sw}) controllers can be defined from Eq. (31) as follows:

$$U_{12\_eq\_SMC} = \frac{C_0 L_0}{V_{dc}} (b_1 x_1 + b_2 x_2 + b_3 x_3) \tag{33}$$

$$U_{12\_sw\_SMC} = -\frac{C_0 L_0}{V_{dc}}\left(k_2 \frac{s_2}{|s_2| + \alpha}\right) \tag{34}$$

Finally,

$$U_{12\_SMC} = \frac{C_0 L_0}{V_{dc}}\left(-R_b k_1 \frac{s_1}{|s_1| + \alpha} + a_1 x_1 + a_2 x_2 + a_3 x_3\right) \quad \text{if CC mode} \tag{35}$$

$$U_{12\_SMC} = \frac{C_0 L_0}{V_{dc}}\left(-k_2 \frac{s_2}{|s_2| + \alpha} + b_1 x_1 + b_2 x_2 + b_3 x_3\right) \quad \text{if CV mode and } S = 1 \tag{36}$$

2.2.2 Integral Sliding Mode Controller (ISMC)

To enhance steady-state accuracy and expedite the convergence of tracking error, ISMC (Integral Sliding Mode Control) is employed. ISMC shares a similar approach to CSMC, differing primarily in the formulation of the sliding surface [27, 28].
CC stage controller design
The sliding surface can be chosen as follows:

$$s_1 = \dot{e}_1 + c_1 e_1 + \int c_3 e_1 \, dt \tag{37}$$

The time derivative of Eq. (37) results in the following expression:

$$\dot{s}_1 = \ddot{e}_1 + c_1 \dot{e}_1 + c_3 e_1 \tag{38}$$

Replacing Eq. (38) into Eq. (15), we obtain:

$$\dot{V}_1 = (\ddot{e}_1 + c_1 \dot{e}_1 + c_3 e_1) s_1 \tag{39}$$

To satisfy the Lyapunov condition $\dot{V}_1 < 0$, it is necessary that:

$$\ddot{e}_1 + c_1 \dot{e}_1 + c_3 e_1 = -k_2 \frac{s_2}{|s_2| + \alpha} \tag{40}$$

By replacing $\ddot{e}_1$ and $\dot{e}_1$ from Eqs. (9) and (10) into Eq. (40), we get:

$$\frac{1}{R_b C_0}\dot{x}_1 + \frac{(c_1 - a)}{R_b}\dot{x}_2 - \frac{(c_1 - b)}{R_b}\dot{x}_3 + c_3 e_1 = -k_2 \frac{s_2}{|s_2| + \alpha} \tag{41}$$

Now, replacing $\dot{x}_1$, $\dot{x}_2$, and $\dot{x}_3$ by these expressions, we obtain the expression of the global sliding mode integral control (U_{12_ISMC}):

$$U_{12\_SMC} = \frac{C_0 L_0}{V_{dc}}\left(-R_b k_1 \frac{s_1}{|s_1| + \alpha} + a_1 x_1 + a_2 x_2 + a_3 x_3 - R_b c_3 e_1\right) \tag{42}$$

Where:

$$\begin{cases} a_1 = \frac{1}{C_0}\frac{r_0}{L_0} - (c_1 - a)\frac{1}{C_0} \\ a_2 = \frac{1}{C_0 L_0} + (c_1 - a)\frac{1}{R_b C_0} + (c_1 - b)\frac{1}{R_b C_b} \\ a_3 = -(c_1 - a)\frac{1}{R_b C_0} - (c_1 - b)\left(\frac{1}{R_b C_b} + \frac{1}{R_P C_b}\right) \end{cases} \tag{43}$$

CV stage controller design
The sliding surface can be selected in the following manner:

$$s_2 = \dot{e}_2 + c_2 e_2 + \int c_3 e_2 \, dt \tag{44}$$

The time derivative of Eq. (44) results in the following expression:

$$\dot{s}_2 = \ddot{e}_2 + c_2\dot{e}_2 + c_4 e_2 \tag{45}$$

Substituting Eq. (45) into Eq. (28), we obtain:

$$\dot{V}_2 = (\ddot{e}_2 + c_2\dot{e}_2 + c_4 e_2)s_2 \tag{46}$$

To satisfy the Lyapunov condition $\dot{V}_2 < 0$, it is necessary that:

$$\ddot{e}_2 + c_2\dot{e}_2 + c_4 e_2 = -k_2\frac{s_2}{|s_2| + \alpha} \tag{47}$$

By substituting $\ddot{e}_2$ and $\dot{e}_2$ from Eqs. (23) and (24) into Eq. (47), we obtain:

$$\frac{1}{C_0}\dot{x}_1 + \left(c_2 - \frac{1}{R_b C_0}\right)\dot{x}_2 + \frac{1}{R_b C_0}\dot{x}_3 + c_4 e_2 = -k_2\frac{s_2}{|s_2| + \alpha} \tag{48}$$

Now, substituting $\dot{x}_1$, $\dot{x}_2$, and $\dot{x}_3$ with these expressions, we obtain the expression for the global sliding mode integral control (U_{12_ISMC}):

$$U_{12\_ISMC} = \frac{C_0 L_0}{V_{dc}}\left(-k_2\frac{s_2}{|s_2| + \alpha} + b_1 x_1 + b_2 x_2 + b_3 x_3 - c_4 e_2\right) \tag{49}$$

The controller parameters k_1, k_2, c_1, c_2, c_3, and c_4 are selected using the empirical method. Where

$$\begin{cases} b_1 = -\left(c_2 - \frac{1}{R_b C_0}\right)\frac{1}{C_0} + \frac{r_0}{C_0 L_0} \\ b_2 = \frac{1}{C_0 L_0} + (c_2 - a)\frac{1}{R_b C_0} \\ b_3 = \frac{1}{R_b C_0}(b - c_2) \end{cases} \tag{50}$$

Finally,

$$U_{12\_SMC} = \frac{C_0 L_0}{V_{dc}}\left(-R_b k_1\frac{s_1}{|s_1| + \alpha} + a_1 x_1 + a_2 x_2 + a_3 x_3 - R_b c_3 e_1\right) \quad \text{if CC mode} \tag{51}$$

$$U_{12\_ISMC} = \frac{C_0 L_0}{V_{dc}}\left(-k_2\frac{s_2}{|s_2| + \alpha} + b_1 x_1 + b_2 x_2 + b_3 x_3 - c_4 e_2\right) \quad \text{if CV mode and } S = 1 \tag{52}$$

2.2.3 Lyapunov stability proof of CSMC and ISMC

To evaluate the overall stability of the system under the first case using conventional sliding mode control, the global Lyapunov function of the system is defined as follows:

$$V_{12} = \frac{1}{2}S_1^2 + \frac{1}{2}S_2^2 \tag{53}$$

The derivative of Eq. (53) with respect to time yields:

$$\dot{V}_{12} = \dot{S}_1 S_1 + \dot{S}_2 S_2 = \dot{V}_1 + \dot{V}_2 \tag{54}$$

Replacing Eqs. (16) and (29) into Eq. (54) results in:

$$\dot{V}_{12} = \left(\frac{1}{R_b C_0}\dot{x}_1 + \frac{(c_1 - a)}{R_b}\dot{x}_2 - \frac{(c_1 - b)}{R_b}\dot{x}_3\right)S_1 + \left(\frac{1}{C_0}\dot{x}_1 + \left(c_2 - \frac{1}{R_b C_0}\right)\dot{x}_2 + \frac{1}{R_b C_0}\dot{x}_3\right)S_2 \tag{55}$$

By replacing $\dot{x}_1$, $\dot{x}_2$, and $\dot{x}_3$ from Eqs. (4), (5), and (6) into Eq. (55), we get:

$$\dot{V}_{12} = \left(-k_1 \frac{s_1}{|s_1| + \alpha}\right) S_1 + \left(-k_2 \frac{s_2}{|s_2| + \alpha}\right) S_2 \leq 0 \tag{56}$$

The same for the ISMC:

$$\dot{V}_{12} = \left(\frac{1}{R_b C_0}\dot{x}_1 + \frac{(c_1 - a)}{R_b}\dot{x}_2 - \frac{(c_1 - b)}{R_b}\dot{x}_3 + c_3 e_1\right) S_1 + \left(\frac{1}{C_0}\dot{x}_1 + \left(c_2 - \frac{1}{R_b C_0}\right)\dot{x}_2 + \frac{1}{R_b C_0}\dot{x}_3 + c_4 e_2\right) S_2 \tag{57}$$

By replacing $\dot{x}_1$, $\dot{x}_2$, and $\dot{x}_3$ from Eqs. (4), (5), and (6) into Eq. (57), we get:

$$\dot{V}_{12} = \left(-k_1 \frac{s_1}{|s_1| + \alpha}\right) S_1 + \left(-k_2 \frac{s_2}{|s_2| + \alpha}\right) S_2 \leq 0 \tag{58}$$

Consequently, the overall asymptotic stability of the system's control laws is ensured.The block diagram for the DC-DC converter is illustrated in Fig. 4. This diagram incorporates measurements of current (ib), voltage (vb), inductor current (iL0), and inner voltage (vc) as inputs to the CC-CV controller blocks. These blocks produce a sinusoidal control signal denoted as "u12," which is subsequently directed to a switching block for selecting the charging step based on the battery voltage level. Finally, a PWM (Pulse Width Modulation) block generates the switching signals (S1 and S2) to regulate the power switches within the converter.

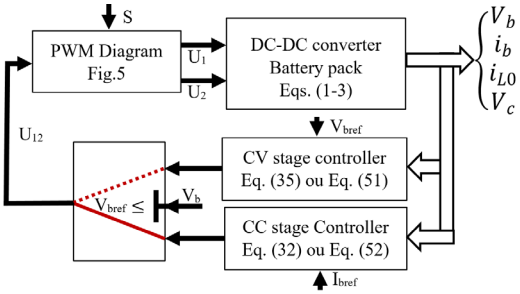

Figure 4. Control Diagram of DC-DC converter

3 Simulation Results

In order to evaluate the efficiency of the controllers designed for the DC-DC power converter, several numerical simulations are carried out using MATLAB/Simulink. The system parameters are detailed in Table 1, and the controller gains are specified in Table 2.

Table 1: The system settings

Description	Parameter	Nominal Value
Capacitor	C_0	700 μF
Inductance	L_0	5 mH
Resistance	r_0	0.1 Ω
Battery Capacitor	C_b	500 F
Series Resistance	R_S	0.006 Ω
Parallel Resistance	R_P	1 kΩ
Battery Voltage	V_b	30 V
Switching Frequency	f_S	20 kHz

Table 2: Parameters of the controllers

PI		CSMC		ISMC	
Parameter	**Value**	**Parameter**	**Value**	**Parameter**	**Value**
K_{1P}	0.1	C_1	1×10^4	C_1	1×10^5
K_{1I}	7	K_1	1×10^6	K_1	1×10^6
K_{2P}	20	C_2	1×10^4	C_2	1×10^4
K_{2I}	10	K_2	1×10^6	K_2	1×10^6
				C_3	1×10^6
				C_4	1×10^{-4}

3.1 Simulation for Grid-to-Vehicle (G2V)

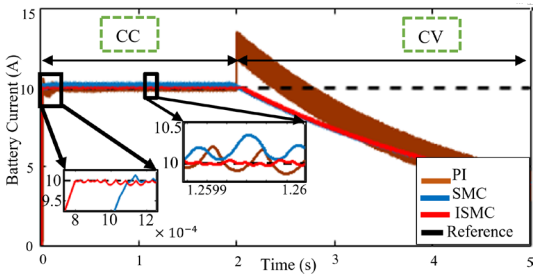

Figure 5. Battery current in G2V mode.

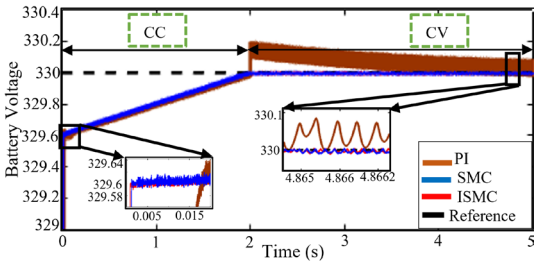

Figure 6. Battery voltage in G2V mode.

The purpose of this section is to assess the performance of the proposed controllers in Grid-to-Vehicle (G2V) mode. Fig. 5 and Fig. 6 illustrate the battery current and voltage under the Constant Current Constant Voltage (CCCV) profile, with reference values set at 10A and 330V.The findings demonstrate that sliding mode control with integral action achieves superior results in terms of both speed and accuracy (refer to Table 3), outperforming conventional sliding mode control and linear PI control methods.

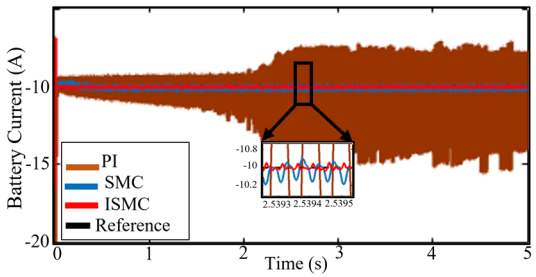

Figure 7. Battery current in V2G mode.

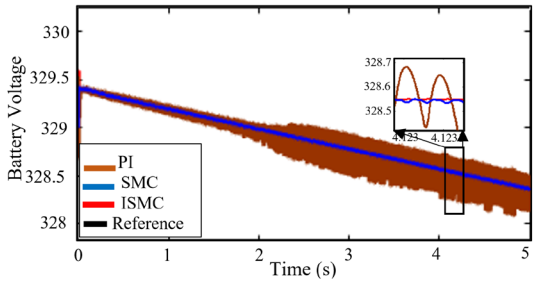

Figure 8. Battery Voltage in V2G mode.

The objective of this section is to assess the effectiveness of the proposed controllers in Vehicle-to-Grid (V2G) mode. Figures 7 and 8 depict the battery current and voltage profiles under the DC profile, with a negative reference value of 10A. The ISMC (Integral Sliding Mode Control) controller demonstrates superior reference tracking and reduced ripple compared to both the SMC (Sliding Mode Control) and PI controllers (refer to Table 3).The PI

controller exhibits significant ripple, highlighting the robustness of non-linear control methods like SMC and ISMC in handling changes in operating points compared to linear control methods.

Table 3: Comparison between the performances of the controllers

Response	PI	CSMC	ISMC
Rise time (s)	0.1	1.114×10^{-3}	8×10^{-4}
Integral of Absolute Error (IAE)	0.3041	0.2668	0.03881
Integral of Time-weighted Absolute Error (ITAE)	0.7637	0.08894	0.0297
Integral of Squared Absolute Error (ISAE)	0.1969	0.2683	0.034
Current ripple (A) in V2G	6.576	0.265	0.1
Current ripple (A) in G2V	0.415	0.374	0.1

Table 3 provides a comparative analysis of the three controller types. According to this comparison, The ISMC controller effectively reduces steady-state error, as shown by calculations from Integral of Absolute Error (IAE), Integral of Squared Absolute Error (ISAE), and Integral of Time-weighted Absolute Error (ITAE). In addition, the SMC and ISMC controllers offer robust performance during transient phases, such as transitions from CC to CV or from Grid-to-Vehicle (G2V) to Vehicle-to-Grid (V2G) modes, compared with the PI controller.

4 Conclusion

This paper provides a detailed comparative study aiming to highlight the distinct differences between sliding mode control (SMC) and emphasize the advantages of the nonlinear approach over classical linear PI control. The study focuses on a system comprising a half-bridge connected to an Electric Vehicle (EV) battery, with primary control objectives centered on ensuring efficient and safe battery charging and discharging. The objectives are substantiated through simulation results, which validate that ISMC, benefiting from its integral action, outperforms both conventional SMC (CSMC) and PI controllers, particularly in terms of speed and accuracy.

References

[1] F. Alanazi, "Electric Vehicles: Benefits, Challenges, and Potential Solutions for Widespread Adaptation," *Applied Sciences*, vol. 13, no. 10, p. 6016, May 2023. https://doi.org/10.3390/app13106016

[2] G. Vishnu, D. Kaliyaperumal, R. Jayaprakash, A. Karthick, V. Kumar Chinnaiyan, and A. Ghosh, "Review of Challenges and Opportunities in the Integration of Electric Vehicles to the Grid," *WEVJ*, vol. 14, no. 9, p. 259, Sep. 2023. https://doi.org/10.3390/wevj14090259

[3] S. Islam, A. Iqbal, M. Marzband, I. Khan, and A. M. A. B. Al-Wahedi, "State-of-the-art vehicle-to-everything mode of operation of electric vehicles and its future perspectives," *Renewable and Sustainable Energy Reviews*, vol. 166, p. 112574, Sep. 2022. https://doi.org/10.1016/j.rser.2022.112574

[4] R. Khezri, D. Steen, and L. Anh Tuan, "Willingness to Participate in Vehicle-to-Everything (V2X) in Sweden, 2022—Using an Electric Vehicle's Battery for More Than Transport," *Sustainability*, vol. 16, no. 5, p. 1792, Feb. 2024. https://doi.org/10.1109/ISGT-Europe54678.2022.9960673

[5] S. Panchanathan et al., "A Comprehensive Review of the Bidirectional Converter Topologies for the Vehicle-to-Grid System," *Energies*, vol. 16, no. 5, p. 2503, Mar. 2023. https://doi.org/10.3390/en16052503

[6] A. Sharma and S. Sharma, "Review of power electronics in vehicle-to-grid systems," *Journal of Energy Storage*, vol. 21, pp. 337–361, Feb. 2019. https://doi.org/10.1016/j.est.2018.11.022

[7] A. Sharma and S. Sharma, "Review of power electronics in vehicle-to-grid systems," *Journal of Energy Storage*, vol. 21, pp. 337–361, Feb. 2019. https://doi.org/10.1016/j.est.2018.11.022

[8] M. Safayatullah, M. T. Elrais, S. Ghosh, R. Rezaii, and I. Batarseh, "A Comprehensive Review of Power Converter Topologies and Control Methods for Electric Vehicle Fast Charging Applications," *IEEE Access*, vol. 10, pp. 40753–40793, 2022. https://doi.org/10.1109/ACCESS.2022.3166935

[9] Z. E. Huma, M. K. Azeem, I. Ahmad, H. Armghan, S. Ahmed, and H. M. M. Adil, "Robust integral backstepping controller for energy management in plugin hybrid electric vehicles," *Journal of Energy Storage*, vol. 42, p. 103079, Oct. 2021. https://doi.org/10.1016/J.EST.2021.103079

[10] A. Phimphui and U. Supatti, "V2G and G2V Using Interleaved Converter for a Single-Phase Onboard Bidirectional Charger," in *2019 IEEE Transportation Electrification Conference and Expo, Asia-Pacific (ITEC Asia-Pacific)*, Seogwipo-si, Korea (South): IEEE, pp. 1–5, May 2019. https://doi.org/10.1109/ITEC-AP.2019.8903662

[11] V. K. Manickam and K. Dhayalini, "Hybrid optimized control of bidirectional off-board electric vehicle battery charger integrated with vehicle-to-grid," *Journal of Energy Storage*, vol. 86, p. 111008, May 2024. https://doi.org/10.1016/j.est.2024.111008

[12] A. Rachid, H. E. Fadil, and F. Giri, "Dual stage CC-CV charge method for controlling DC-DC power converter in BEV charger," in *2018 19th IEEE Mediterranean Electrotechnical Conference (MELECON)*, Marrakech: IEEE, pp. 74–79, May 2018. https://doi.org/10.1109/MELCON.2018.8379071

[13] S. Ghosh, A. K. Singh, R. Singh, R. Maurya, S. N. Singh, and G. Yang, "Intelligent control of integrated on-board charger with improved power quality and reduced charging transients," *ISA Transactions*, vol. 135, pp. 355–368, Apr. 2023. https://doi.org/10.1016/j.isatra.2022.10.005

[14] A. Zar, H. Rehman, and I. Ahmad, "Neural network based optimized barrier conditioned double super-twisting sliding mode controller of electric vehicle charger with grid to vehicle and vehicle to grid modes," *Journal of Energy Storage*, vol. 74, p. 109234, Dec. 2023. https://doi.org/10.1016/j.est.2023.107251

[15] U. Masood, M. K. Azeem, I. Ahmad, and A. U. Jabbar, "Robust adaptive nonlinear control of plugin hybrid electric vehicles for vehicle to grid and grid to vehicle power flow with hybrid energy storage system," *ISA Transactions*, vol. 139, pp. 406–424, Aug. 2023. https://doi.org/10.1016/j.isatra.2023.03.035

[16] H. Lin *et al.*, "Integral Sliding-Mode Control-Based Direct Power Control for Three-Level NPC Converters," *Energies*, vol. 13, no. 1, p. 227, Jan. 2020. https://doi.org/10.3390/en13010227

[17] K. Oualifi, H. Abouobaida, Y. Mchaouar, Y. Abouelmahjoub, D. Elmesouli, and A. Fathelkhair, "Comparative Study of Conventional Sliding Mode Control and Sliding Mode with Integral Action in an Electric Vehicle Charger Application," in *Automatic Control and Emerging Technologies, ACET 2023*, El Fadil, H., Zhang, W. (eds), 2024. https://doi.org/10.1007/978-981-97-0126-1_58

[18] H. M. Mehdi, M. K. Azeem, and I. Ahmad, "Artificial intelligence based nonlinear control of hybrid DC microgrid for dynamic stability and bidirectional power flow," *Journal of Energy Storage*, vol. 58, p. 106333, Feb. 2023. https://doi.org/10.1016/j.est.2022.106333

[19] A. Sharma and S. Sharma, "Review of power electronics in vehicle-to-grid systems," *Journal of Energy Storage*, vol. 21, pp. 337–361, Feb. 2019. https://doi.org/10.1016/j.est.2018.11.022

[20] V. Viswanatha, A. C. Ramachandra, and R. Venkata Siva Reddy, "Bidirectional DC-DC converter circuits and smart control algorithms: a review," *Journal of Electrical Systems and Information Technology*, vol. 9, no. 1, p. 6, Apr. 2022. https://doi.org/10.1186/s43067-022-00048-z

[21] M. C. Annamalai and N. Amutha Prabha, "A comprehensive review on isolated and non-isolated converter configuration and fast charging technology: For battery and plug-in hybrid electric vehicle," *Heliyon*, vol. 9, no. 8, p. e18808, Aug. 2023. https://doi.org/10.1016/j.heliyon.2023.e18808

[22] G. Saldaña, J. I. San Martín, I. Zamora, F. J. Asensio, and O. Oñederra, "Analysis of the Current Electric Battery Models for Electric Vehicle Simulation," *Energies*, vol. 12, no. 14, p. 2750, Jul. 2019. https://doi.org/10.3390/en12142750

[23] A. Garg, X. Peng, M. L. P. Le, K. Pareek, and C. M. M. Chin, "Design and analysis of capacity models for Lithium-ion battery," *Measurement*, vol. 120, pp. 114–120, May 2018. https://doi.org/10.1016/J.MEASUREMENT.2018.02.003

[24] C. Napole, M. Derbeli, and O. Barambones, "A global integral terminal sliding mode control based on a novel reaching law for a proton exchange membrane fuel cell system," *Applied Energy*, vol. 301, p. 117473, Nov. 2021. https://doi.org/10.1016/j.apenergy.2021.117473

[25] A. Rachid, H. El Fadil, F. Giri, and A. Lassioui, "Nonlinear output feedback control of V2G single-phase on-board BEV charger," *Asian Journal of Control*, vol. 22, no. 5, pp. 1848–1859, Sep. 2020. https://doi.org/10.1002/asjc.2082

[26] S. Joyce Pinto, "Design and Performance of Vehicle to Grid Integration with DG Infrastructure," *PETPES*, 2019. https://doi.org/10.1109/PETPES47060.2019.9003919

[27] A. Kihal, F. Krim, B. Talbi, A. Laib, and A. Sahli, "A Robust Control of Two-Stage Grid-Tied PV Systems Employing Integral Sliding Mode Theory," *Energies*, vol. 11, p. 2791, 2018. https://doi.org/10.20944/PREPRINTS201808.0458.V1

[28] H. Lin, J. I. Leon, W. Luo, A. Marquez, J. Liu, S. Vazquez, and L. G. Franquelo, "Integral Sliding-Mode Control-Based Direct Power Control for Three-Level NPC Converters," *Energies*, vol. 13, p. 227, Jan. 2020. https://doi.org/10.3390/en13010227